

钛合金(TC4)电子束焊接模拟

曾庆继¹, 徐连勇^{1,2}, 韩永典^{1,2}, 荆洪阳^{1,2}, 周春亮³

(1. 天津大学材料学院,天津 300072; 2. 天津市现代连接技术重点实验室,天津 300072;
3. 中国电子科技集团第18研究所,天津 300381)

摘 要: 通过工艺试验,获得了9 mm厚 TC4 电子束焊接最佳工艺参数;利用有限元软件 ABAQUS 建立模型. 结果表明,模拟焊缝形貌和表面残余应力结果与实测结果具有非常高的一致性,说明了穿透性强的圆锥热源和辐射性强的双椭圆热源组成的复合热源能够有效地反应出电子束焊接特点,证明了有限元模型的正确性;进而对模拟结果进一步分析,得到焊缝周围存在较高残余应力,尤其是在焊件内部存在危险的三维拉伸应力状态.

关键词: 电子束焊接; 钛合金; 有限元模拟; 残余应力; 复合热源

中图分类号: TG 456.3 文献标识码: A 文章编号: 0253-360X(2014)11-0109-04

0 序 言

电子束焊接具有能量密度高、纯净度高、热影响区小、高度自动化等一系列优点,在航空航天等领域成为钛合金焊接的首选. 而电子束焊接是一个快速而极不均匀的热循环过程,焊缝周围附近会出现较大的温度梯度分布,因此在焊后结构中会出现不同程度的残余应力和变形,焊接残余应力和变形可能引起裂纹甚至脆性断裂而影响焊接结构的质量和性能^[1]. 对焊接温度场、应力和变形的分析以往都是通过试验方法测量并采集数据,进行定量的分析. 在计算机技术日益发展的今天,采用数值模拟的方法来模拟复杂的焊接现象取得了很大的进展^[2]. 文献[3]对6 mm厚的TC11平板进行了不同电子束焊接工艺参数下的应力模拟,得到正面焊透加背面修饰可以降低纵向残余应力;西北工大胡美娟^[4]利用ANSYS软件对12 mm厚TC4钛合金电子束焊接的温度场和应力场进行了模拟,并与试验测量结果进行对比,得出板件中心存在危险的三维残余拉应力状态. 大多研究者对钛合金的模拟主要是考虑应力分布是否与实际相符,而对焊缝形貌,尤其是焊缝余高是否准确未见系统深入的报道.

文中,研究以9 mm厚的TC4钛合金平板对接焊为研究对象,通过工艺试验确定焊接参数后,利用ABAQUS软件模拟焊接过程,并将计算应力和焊缝形貌结果同实测结果进行比较,以便对实际焊接工艺的制定和进一步消除残余应力打下基础.

1 焊接方法

试验选用9 mm厚的TC4钛合金,供货状态热轧、退火,材料成分如表1. 采用平板对接,平板尺寸120 mm × 100 mm × 9 mm. 电子束设备选用法国TECHMETA真空电子束焊机. 试验前,对平板采用酒精+超声清洗,防止油污、水分等污染焊接接头. 紧密装配平板焊件,选择焊接速度1 m/min,调节聚焦电流、电压和电子束电流进行焊接工艺研究. 试验参数及焊缝形貌结果见表2. 可见I组焊缝形貌最佳,焊缝正反面如图1所示. 得出9 mm厚TC4钛合金电子束焊接最佳工艺参数见表3.

表1 TC4化学成分(质量分数,%)

Table 1 Chemical compositions of TC4

Al	V	Fe	Si	C	N	H	O	Ti
6.06	3.92	0.3	0.15	0.01	0.05	0.0015	0.2	余量

表2 TC4电子束焊接工艺试验

Table 2 EBW process experiments of TC4

分组	电压 U/kV	聚焦电流 I _f /mA	电子束流 I _b /mA	焊缝形貌
A	40	50	2 050	未焊透
B	40	80	2 050	未焊透
C	40	120	2 050	未焊透
D	60	80	2 550	焊缝塌陷
E	60	60	2 550	焊缝塌陷
F	60	50	2 550	焊缝塌陷
G	60	40	2 550	焊缝部分塌陷
H	60	30	2 550	未焊透
I	60	36	2 550	焊缝形态良好



图 1 I 组焊缝形貌

Fig. 1 Weld profile of group I

表 3 电子束焊接最佳工艺参数

Table 3 Optimum process parameters of EBW

聚焦电流 I_f/mA	电压 U/kV	电子束电流 I_b/mA	焊接速度 $v/(\text{m}\cdot\text{min}^{-1})$
2 550	60	36 ~ 40	1

2 数值模拟

2.1 理论基础

电子束焊接过程属于典型的非线性瞬态热传导问题. 三维非线性瞬态热传导方程为

$$\rho c = \frac{\partial}{\partial x} \left(\lambda \frac{\partial T}{\partial x} \right) + \frac{\partial}{\partial y} \left(\lambda \frac{\partial T}{\partial y} \right) + \frac{\partial}{\partial z} \left(\lambda \frac{\partial T}{\partial z} \right) + \bar{Q} \quad (1)$$

式中: ρ 、 c 和 λ 分别是材料的密度、比热容和导热系数; \bar{Q} 为内热源强度^[1]. 焊接应力和变形计算的理论基础是弹塑性有限元理论.

2.2 热源模型

据文献[6]焊接过程中,高速电子撞击金属表面形成高温金属蒸汽. 而熔池表面高温金属蒸汽会对液态金属传热,且因具有一定压强而呈现椭球形貌. 因而选取锥形体热源和双椭球热源的复合热源. 圆锥和双椭球形热源模型如图 2 所示: 锥形在 z 轴各处的截面均为圆,随着 z 值的不断增大,半径减小. 因此,圆锥形体热源能够描述小孔半径在深度方向的衰减规律;双椭球热源能够体现椭球形高温蒸汽对熔池的加热作用. 锥形和双椭球体热源在任一点热流表达式分别为

$$q_1(r, z) = \frac{9f_1\Phi}{\pi hr_0^2} e^{-\frac{3h^2}{(h+z)^2 r_0^2} (x^2 + y^2)} \quad (2)$$

$$q_2(r, z) = \frac{6\sqrt{3}f_2\Phi}{abc\pi^{\frac{3}{2}}} e^{-3\left(\frac{x^2}{a^2} + \frac{y^2}{b^2} + \frac{z^2}{c^2}\right)} \quad (3)$$

式中: Φ 为焊接有效功率; f_1 、 f_2 为热流密度分布系数; r_0 为圆锥表面半径; r 为任一截面半径; h 为圆锥高度; a 、 b 、 c 为椭球形状参数.

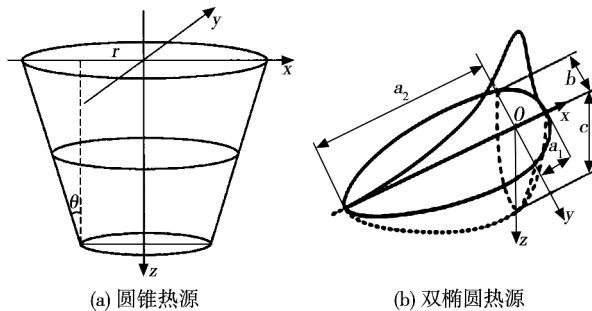


图 2 热源示意图

Fig. 2 Schematic diagram of heat source

2.3 有限元模型的建立

由于平板对称性,取其一半(100 mm × 60 mm × 9 mm)进行建模分析. 网格划分时,考虑到电子束的聚焦束斑直径约为 0.5 mm,焊缝附近采用较小的网格尺寸 0.5 mm × 0.5 mm. 温度场计算采用网格类型为 DC3D8,应力场为 C3D8R. 文中采用顺序耦合场分析,即首先进行温度场计算,然后计算应力场时调用温度场结果进行热弹塑性应力分析. 焊接过程中,TC4 钛合金 0 ~ 500 °C 的热力学材料数据由文献[5]得到,对更高温段数据采用线性拟合并通过插值和外推的方法得到. 整个焊接过程都是在真空中进行,热量的散失只有焊件表面辐射散热. 在应力场计算中,焊缝中心截面采取对称约束,底面约束三个顶点,使平板在 x 、 y 方向上不能自由移动.

2.4 有限元计算结果

2.4.1 温度场计算结果分析

整个求解计算过程分为焊接和冷却两个阶段. 焊接过程在 6.25 s 内完成,冷却时间为 3 000 s. 计算过程中载荷步的选择由程序进行自适应控制,即焊接过程非线性较强,适当减小步长,而冷却过程在保证计算精度的前提下,适当增大步长. 热载荷采用 Fortran 语言编写并作为子程序方式调用进行计算. 冷却后整块平板温度为 33 °C 左右,但平板内温差已经相当小,对焊后应力和变形的影响可忽略,此时应力计算结果可以作为最后应力和变形分布.

距焊缝中心 0、0.6、1.825 和 2.875 mm 处各节点的温度循环曲线如图 3 所示;计算熔池形貌与焊缝形貌对比如图 4 所示;计算焊缝余高如图 5 所示.

图 3 得出:电子束束斑到达焊缝中心时,焊缝附近温度迅速上升,最高温度在 3 750 °C 以上. 距离焊缝中心越远,温度上升越慢,并且所能达到的最高温

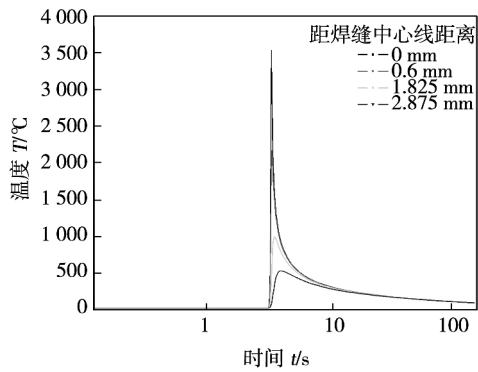


图 3 热循环曲线
Fig. 3 Thermal cycling curve

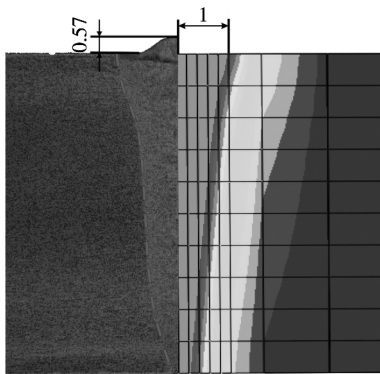


图 4 计算熔池与焊缝对比(mm)
Fig. 4 Contrast of calculated pool and weld profile

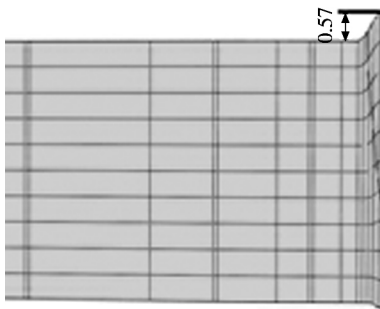


图 5 计算焊缝余高(mm)
Fig. 5 Calculated weld reinforcement

度迅速下降. 如距焊缝中心 0.6 mm 处, 最高温度达 2 400 °C, 距焊缝中心 3 mm 附近最高温只有 500 °C 左右. 由此可以估算靠近焊缝处温度差高达 2 250 °C/mm. 当束斑离开后, 焊缝中心温度迅速下降, 而远离焊缝中心的温度仍有所升高, 但随后也会缓慢下降. 随着时间的推移, 整个平板的温度趋于均匀.

图 4, 图 5 得出: 计算焊缝形状尺寸与实际焊缝一致. 实测焊缝宽度在 1.9 ~ 2.1 mm 之内, 计算焊缝宽度为 2.0 mm, 两者基本相等; 实测焊缝余高在 0.55 ~ 0.58 mm 之内, 计算结果为 0.57 mm, 与实测结果基本相符.

2.4.2 应力场计算结果分析

冷却后平板等效应力分布如图 6 所示. 利用盲孔法(选用直径 1.5 mm 钻头, 钻取深度 1.6 mm)对焊后 TC4 平板垂直焊缝表面上多点(图 7)应力进行了测量, 并与计算结果对比. 纵向应力和横向应力对比分别如图 8, 图 9 所示; 焊缝中心线(路径 2)表面纵向和横向残余应力计算结果如图 10 所示; 焊缝中心沿厚度方向(路径 3)应力分布如图 11 所示.

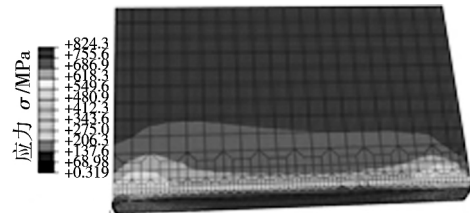


图 6 等效残余应力分布
Fig. 6 Equivalent residual stress distribution

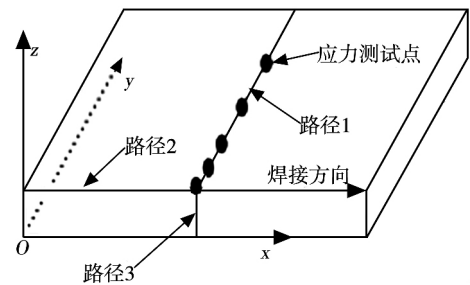


图 7 应力测试点与模拟结果路径
Fig. 7 Test points and simulation results path

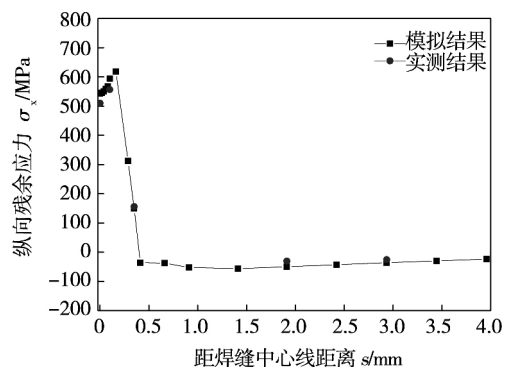


图 8 垂直焊缝中心线上纵向残余应力
Fig. 8 Longitudinal stress on vertical weld line

图 6 得出: 在距离焊缝中心线 2 mm 区域内, 存在着较大的等效应力, 最大应力存在于平板焊缝中心截面处, 高达 820 MPa, 接近 TC4 钛合金的屈服强度(920 MPa). 随距焊缝中心越远, 应力值迅速降低. 距焊缝中心 3.5 mm 处等效应力为 140 MPa 左右. 这表明巨大的温差导致较大残余应力, 且主要集中在距焊缝 4 mm 区域内.

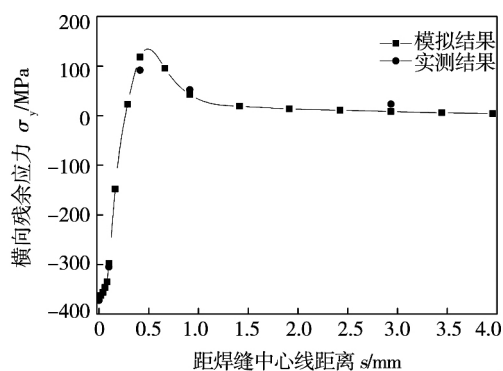


图9 垂直焊缝中心线上横向残余应力

Fig. 9 Transverse stress on vertical weld line

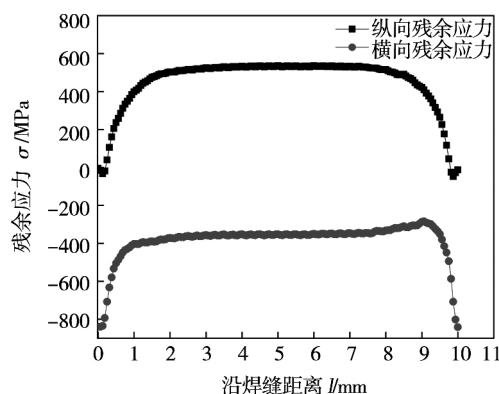


图10 焊缝中心表面纵向和横向残余应力

Fig. 10 Stresses of weld center

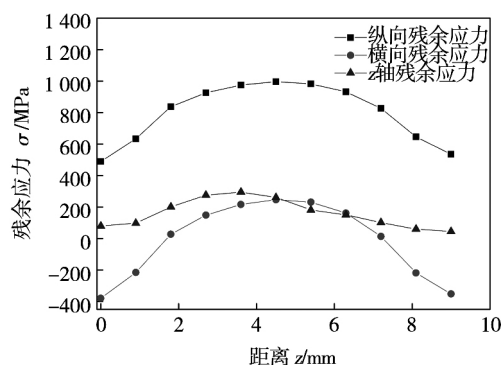


图11 焊缝中心厚度方向残余应力

Fig. 11 Stress in thickness of weld center

图8,图9得出:焊缝表面残余应力模拟结果和实测结果一致.纵向残余应力在焊缝及近缝区为较高数值的拉应力,最大接近600 MPa;距焊缝中心越远数值迅速下降,并转变为压应力,达到最大压应力后又逐渐升高至零.图10显示焊缝中心表面纵向残余应力在起始和收尾端较小,中间区域拉应力值基本保持稳定,且数值接近600 MPa.这是由于平板两端可以自由变形,中间区域受到夹具和平板自身的拘束作用而产生较大的拉伸应力;横向应力由于

受到纵向伸长而受到压缩表现为压应力,最大达到-350 MPa.距焊缝中心线远处,压应力值迅速减小并变为拉应力,随后趋于零.

图11得出:厚度方向上各点(路径3)纵向残余应力为拉应力,横向残余应力两端为压应力,中间为拉应力,厚度方向为拉应力;焊缝内部存在三向拉伸应力.造成焊缝中间区域横向残余应力在表面受压内部受拉的原因是表面先熔化的区域在冷却过程中受到后熔化区域的膨胀作用而产生了压应力;平板内部熔池凝固收缩被未熔化区域阻止而产生拉应力.

3 结 论

(1) 通过焊接试验,得到9 mm厚TC4钛合金电子束焊接最佳工艺参数.

(2) 通过模拟结果与实测结果对比,证明圆锥与双椭球复合热源选择和有限元模型的准确性.

(3) 中厚焊件电子束焊接后在焊缝内部存在着较大残余应力,尤其是在焊缝内部存在三向拉伸状态.

参考文献:

- [1] 王西昌,左从进,刘方军,等.基于SYSWELD软件的TC4电子束焊接过程的数值模拟[J].新技术新工艺,2007(1):8-11. Wang Xichang, Zuo Congjun, Liu Fangjun. Numerical simulation of the EBW of TC4 alloy plate based on SYSWELD [J]. New Technology & New Process, 2007(1): 8-11.
- [2] 李林贺,陈芙蓉,郭桂芳.电子束焊接数值模拟技术的研究进展[J].造船技术,2001,242(4):21-24. Li Linhe, Chen Furong, Guo Guifang. Research progress of numerical simulation in electron beam welding [J]. Inner Mongolia Petrochemical Industry, 2001, 242(4): 21-24.
- [3] 刘敏,陈士焯,康继东,等.钛合金平板电子束焊接残余应力数值分析[J].航空动力学报,2001(1):63-66. Liu Min, Chen Shixuan, Kang Jidong, et al. Numerical model for the temperature and stress fields of moving EBW in titanium alloy plates [J]. Journal of Aerospace Power, 2001(1): 63-66.
- [4] 胡美娟,刘金合.12 mm厚钛合金平板电子束焊接的数值模拟[J].中国有色金属学报,2007,17(10):39-42. Hu Mei Juan, Liu Jin He. Numerical simulation for electron beam welding of 12 mm-thickness titanium alloy plate [J]. The Chinese Journal of Nonferrous Metals, 2007, 17(10): 39-42.
- [5] 于慧臣,吴学仁.航空发动机设计用材料数据手册:第四册[M].北京:中国标准出版社,2010.
- [6] Martin B, Loredo A, Pilloz M, et al. Characterisation of cw Nd:YAG laser keyhole dynamics [J]. Optics & Laser Technology, 2001, 33(4): 201-207.
- [7] Ji Zhong, Wu Shichun. FEM simulation of the temperature field during the laser forming of sheet metal [J]. Journal of Materials Processing Technology, 1998, 74(1): 89-95.

作者简介:曾庆继,男,1988年出生,硕士研究生.研究方向为金属材料电子束焊接工艺及模拟技术.发表论文1篇. Email: zengqing_ji@126.com

通讯作者:徐连勇,男,副教授. Email: xulianyong@tju.edu.cn

Abstract: In order to understand the corrosion resistance of different materials surfaces machined by micro wire electrical discharge machining (MWEDM) , the specimens of three kinds of materials ,including W18Cr4V ,60Si2Mn and M42 ,were separately processed. The micro electrolytic cell equipment and electrochemical workstation were applied to test the corrosion resistance of specimen surfaces , and the electrochemical impedance spectroscopy and potentiodynamic polarization curves were measured and analyzed. Besides , the surfaces after corrosion were observed with inverted metallurgical microscope , and were compared to flat grinding surfaces. The results showed that corrosion resistance of MWEDM surfaces was superior to that of flat grinding surfaces. For different materials , corrosion resistance of MWEDM surfaces was significantly different from each other. For the same material , the surface with better corrosion resistance could be obtained by using appropriate processing parameters.

Key words: micro wire electrical discharge machining; corrosion resistance; electrochemical impedance spectroscopy; potentiodynamic polarization curve

Using dynamic induction heating to inhibit martensite structure formed in heat-affected zone of U71Mn steel rail after surface welding YAN Wentao , LI Xiaoyan , LI Hui , SUN Jiantong (School of Material Science and Engineering , Beijing University of Technology , Beijing 100124 , China) . pp 97 - 100 , 108

Abstract: A dynamic induction heating method was used to inhibit the formation of martensite in heat-affected zone (HAZ) of U71Mn steel rail after surface welding. The inhibition of martensite structure was characterized by optical microstructure analysis and microhardness testing. The experimental results showed that when the U71Mn steel rail was welded in cold welding condition , cracks would form directly in the heat-affected zone , and the microstructure was martensite. With the increase of preheating and post-heating temperature , the amount of martensite reduced significantly. When the preheating temperature was 320 °C and post-heating temperature was 550 °C , the martensite structure could be inhibited completely , and the heat-affected zone consisted of sorbite structure whose size was smaller than pearlite structure in the base metal. The microhardness of the heat-affected zone also distributed uniformly.

Key words: dynamic induction heating; U71Mn steel rail; surface welding; martensite

Arc pressure analysis in variable polarity TIG welding

CHENG Lin , HU Shengsun , WANG Zhijiang (Tianjin Key Laboratory of Advanced Joining Technology , Tianjin University , Tianjin 300072 , China) . pp 101 - 104

Abstract: The arc pressure during horizontal variable polarity gas tungsten arc welding (VPTIG) was measured by pressure transducer under different welding conditions. The radial distribution of arc pressure was investigated , and the central arc pressures for DC TIG welding and VPTIG welding with a period of 5% and 15% for direct current electrode positive (DCEP) were compared. The experimental results showed that the radial

distribution of VPTIG pressure was hyperbolic. When the welding current was in the range of 100 A to 140 A and with the same root mean square value , the arc pressure decreased gradually with the increase of time ratio of DCEP at one cycle during DC TIG welding and VPTIG welding with a period of 5% and of 15% for DCEP , due to the difficulties of electron emission and arc divergence in the period of DCEP. And the integrated arc force was directly proportional to the square of welding current.

Key words: hyperbolic distribution; arc pressure; horizontal welding; variable polarity gas tungsten arc welding

Effect of hot-cutting defect on reliability of brazing process in ceramic package manufacturing—II. Brazing structure design

ZENG Chao , WANG Chunqing , TIAN Yanhong , ZHANG Wei (State Key Lab of Advanced Welding and Joining , Harbin Institute of Technology , Harbin 150001 , China) . pp 105 - 108

Abstract: Reliability of brazing process in ceramic package manufacturing depends on the interaction between thermal stress induced by mismatch of CTE (coefficient of thermal expansion) and defect in ceramic generated in the process before brazing. This paper based on the feature that defects with different degrees of danger spatially locate differently , and employed ANSYS software to analyze the distribution of the thermal stress in brazing process. A novel idea of avoiding the stress locating at defect region was applied to improve the reliability of assembly process. This idea is different from the traditional optimizing method to lowering the stress over the whole component , and is more flexible for the package design , and it is also more effective for improving the reliability of ceramic package manufacturing.

Key words: thermal mismatch; package structure; process reliability

Finite element numerical simulation of electron beam welding of TC4 titanium alloy

ZENG Qingji¹ , XU Lianyong^{1,2} , HAN Yongdian^{1,2} , JING Hongyang^{1,2} , ZHOU Chunliang³ (1. School of Materials Science and Engineering , Tianjin University , Tianjin 300072 , China; 2. Tianjin Key Laboratory of Advanced Joining Technology , Tianjin 300072 , China; 3. The 18th Research Institute of CETC , Tianjin 300381 , China) . pp 109 - 112

Abstract: The optimized welding parameters for electron beam welding of 9 mm thick TC4 titanium alloy plate were obtained. A finite element model was established based on ABAQUS software , and the simulated results of the weld appearance and residual stress on the weld surface agreed well with the experimental results. This proved that the combined heat source with highly penetrating cone heat source and highly irradiative dual-ellipsoid heat source could characterize the electron beam welding. Further simulated results showed that high residual stress occurred around the weld , especially , dangerous three-dimensional tensile stress existed within the weldment.

Key words: electron beam welding; TC4 titanium; finite element numerical simulation; residual stress; composite heat source